Sensitivity analysis of design parameters for melting process of lauric acid in the vertically and horizontally oriented rectangular thermal storage units

Safari, Vahid; Kamkari, Babak; Hooman, Kamel; Khodadadi, J. M.

DOI
10.1016/j.energy.2022.124521

Publication date
2022

Document Version
Final published version

Published in
Energy

Citation (APA)
Safari, V., Kamkari, B., Hooman, K., & Khodadadi, J. M. (2022). Sensitivity analysis of design parameters for melting process of lauric acid in the vertically and horizontally oriented rectangular thermal storage units. *Energy*, *255*, Article 124521. https://doi.org/10.1016/j.energy.2022.124521

Energy 255 (2022) 124521

Contents lists available at ScienceDirect

Energy

journal homepage: www.elsevier.com/locate/energy

Sensitivity analysis of design parameters for melting process of lauric acid in the vertically and horizontally oriented rectangular thermal storage units

Vahid Safari [a], Babak Kamkari [b, e, *], Kamel Hooman [c], J.M. Khodadadi [d]

[a] Center for Separation Processes Modeling and Nano-Computations, School of Chemical Engineering, College of Engineering, University of Tehran, Tehran, Iran
[b] Department of Mechanical Engineering, Yadegar-e-Imam Khomeini (RAH) Shahre-Rey Branch, Islamic Azad University, Tehran, Iran
[c] Delft University of Technology, Process and Energy Department, Leeghwaterstraat 39, 2628 CB, Delft, Netherlands
[d] Mechanical Engineering Department, Auburn University, 1418 Wiggins Hall, Auburn, AL, 36849-5341, USA
[e] Centre for Sustainable Technologies, Belfast School of Architecture and the Built Environment, Ulster University, Northern Ireland, UK

ARTICLE INFO

Article history:
Received 11 January 2022
Received in revised form
21 May 2022
Accepted 11 June 2022
Available online 14 June 2022

Keywords:
Latent heat storage
Phase change materials (PCM)
Natural convection
Heat transfer

ABSTRACT

Widespread commercialization of PCM-based latent heat storage systems is limited by the low melting and solidification rates during the phase transition process. In this study, fins are used to enhance the phase change process. A parametric study is conducted to understand the effect of fins on the thermal performance of vertically- and horizontally-oriented rectangular storage tanks. Throughout simulations, the fin volume, and thereby the mass of PCM in the tank, were kept constant. It was observed that the horizontal enclosures can take advantage of the development of strong natural convection flow until near the end of the melting process, whereas with vertical counterparts the strength of the convection currents was diminished during the shrinkage stage. The results suggest that longer and thinner fins are more beneficial for enhancing the melting rate than shorter and thicker fins. It was concluded that for horizontal enclosures with fin lengths of 25 and 35 mm, increasing the number of fins does not necessarily shorten the melting time. The maximum melting time reduction compared to the 3-fin vertical enclosure with a fin length of 25 mm (chosen as our benchmark case) was 75.1% when nine 45-mm-long fins are used in a horizontal enclosure.

1. Introduction

Over the last decade, there has been a renewed interest in latent heat thermal storage systems (LHTS) based on phase change materials (PCM) due to the massive capacity of storing thermal energy at isothermal conditions [1,2]. Moreover, commercial availability at a competitive cost and wide melting temperature range make PCM favorable in different applications including solar energy systems [3,4], thermal management of batteries [5,6], energy-savings in buildings [7,8], cold storage [9,10], hot water systems [11,12], air conditioning [13,14], and food industry [15,16]. However, the low thermal conductivity of PCM is the main drawback that limits their extensive usage in practical applications [17]. Employing metal foams [18,19], nanoparticles [20,21], extended surfaces [22–24] are some of the most investigated thermal conductivity enhancement techniques for PCM-based systems. In addition, the shape of the storage tank is another key parameter that can significantly influence the melting rate of the PCM [25]. Rectangular [26,27], shell and tube [28,29] and spherical [30,31] tanks are tested as current industry practice. This research focuses on the melting enhancement of PCM in finned rectangular geometries which are commonly used as heat sinks for electronic cooling [32,33]. Abdi et al. [34] conducted a numerical study to understand the effect of straight fins on melting rate improvement of the lauric acid PCM in horizontal rectangular storage tanks. They reported that the 5-fins enclosure with dimensionless fin length of 0.75 exhibited the best melting performance with melting time reduction and mean thermal power enhancement of 77% and 200%, respectively, compared with the no-fin case. Nakhchi and Esfahani [35] numerically studied the effect of stepped fins on the melting

* Corresponding author. Department of Mechanical Engineering, Yadegar-e-Imam Khomeini (RAH) Shahre-Rey Branch, Islamic Azad University, Tehran, Iran.
E-mail address: kamkari@ut.ac.ir (B. Kamkari).

https://doi.org/10.1016/j.energy.2022.124521
0360-5442/

Nomenclature

A	heat transfer area (m^2)
C_p	specific heat capacity (J/ kg.K)
D	depth of the container, (mm)
d	fin spacing, (mm)
g	gravitational acceleration (m/ s^2)
H	height of the container, (mm)
h	enthalpy (J/kg)
k	thermal conductivity (W/m.K)
L	fin length (mm)
l	latent heat of fusion (J/kg)
P	pressure (Pa)
q	instantaneous heat transfer rate (J/s)
$\vec{S}$	source term
t	thickness of the fin, (mm)
T	temperature (°C)
u	horizontal velocity component (m/s)
v	vertical velocity component (m/s)
$\vec{V}$	velocity vector (m/s)
W	width of the container, (mm)

Abbreviations

HTF	heat transfer fluid
LHTS	latent heat thermal storage
LHSU	latent heat storage unit
MER	melting enhancement ratio
PCM	phase change materials

Greek symbols

β	thermal expansion coefficient (1/K)
γ	melt fraction
μ	dynamic viscosity (kg/ m.s)
ν	kinematic viscosity (m^2/ s)
ρ	mass density (kg/ m^3)

Subscripts

avg	average
c	container
f	fin
init	initial
lat	latent
m	melting
ref	references
s	solid
sens	sensible
tot	total
w	wall

process in a laterally-heated rectangular tank. Results showed that melting is enhanced by increasing the step ratio and that setting the fins downward led to better performance compared with the upward case. It was also reported that the highest melting rate improvement at optimized downward stepped fins is about 65.5% faster than the conventional 3-fins storage units. Kalbasi et al. [36] carried out a parametric study to find the optimal fin numbers in a PCM-based rectangular heat sink. A tank with thin and tall fins was recommended as the optimal design configuration. Applying the Response Surface Method (RSM), a similar optimization study was conducted by Zhao et al. [36] for a shell and tube latent heat storage units. Aiming at shortening the melting time, an optimum fin number density, subject to a specific fin volume constraint, was reported. Kamkari and Shokouhmand [37] conducted an experimental research to examine the impact of horizontal fins on the heat transfer rates of lauric acid filling a vertical rectangular storage tank. The results indicated that the melting time for the 1-fin and 3-fins units were reduced up to 18% and 37%, respectively, compared with the no-fin enclosure. However, it was concluded that increasing the number of fins leads to a decremental trend for the Nusselt number. Ji et al. [38] performed a numerical study to analyze the effect of the fin length, and inclination angles on the melting process of the paraffin (RT42) in a laterally-heated rectangular box. It was noted that tilted fins with a downward inclination angle of -15° suppresses the non-uniform melting pattern in the cavity and reduce the melting time by up to 62.7% compared with the no-fin case. In a subsequent study, Ji et al. [39] studied the impact of double-fin configurations with a longer fin at the bottom of the rectangular LHSU. It was reported that the strength of the convection currents could be improved by decreasing the length ratio of the higher fin to the lower one. Results showed that the optimal ratio was 0.11 with a melting time reduction of 40%. Hosseinizadeh et al. [40] studied the cooling performance of PCM-based finned heat sinks numerically and experimentally. The impacts of different parameters like the number, length, and thickness of the fins and the impact of the power inputs were studied in detail. Considerable enhancement of the thermal performance was reported when the number density and height of the fins were increased. However, increasing the fin thickness was found to only marginally impact the melting rate. Biwole et al. [41] numerically investigated the influence of the number density and configurations of horizontal fins on the melting process of a PCM tank heated subject to a constant heat flux on the side wall. Weaker convective patterns were observed with higher fin number density values. Similar observations were made by Kamkari and Karami [42].

While a great deal of information is available in the literature, as briefly surveyed here, only a handful of the above papers compared different cases (with or without fins) subject to the same mass of PCM constraint. To the best of our knowledge, this is the first combined numerical and experimental research that compares the performance of vertical and horizontal rectangular storage tanks with fins subject to this constraint, i.e., the mass of PCM or the volume of fins is kept constant in each run. Accordingly, the effects of fins' length, number density, and thickness on the phase change process are investigated.

2. Problem statement and physical model

The main aim of this study is to investigate the effect of the fins' number density, length, and thickness on the melting rate of PCM in vertical and horizontal rectangular latent heat storage units (LHSU). The rectangular tank is heated on one wall while the other walls are insulated. Fig. 1(a) shows the photograph of the aluminum (Alloy 5052) finned heat exchanger prepared by Computer Numerical Control (*CNC) machining* with positioning accuracy of 0.010 mm for providing the isothermal boundary condition on the side wall of the enclosure. This was accomplished by passing the hot water through the holes of the heat exchanger. The description of the employed experimental apparatus and the test procedure can be found in Kamkari et al. [43]. Fig. 1(b) illustrates the schematic diagram of the

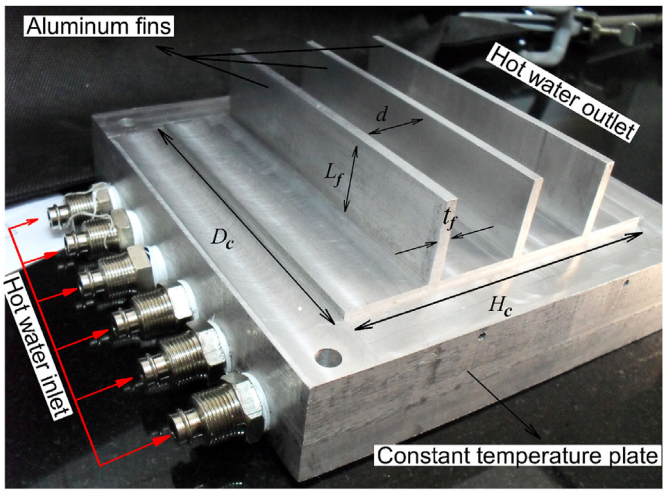

(a)

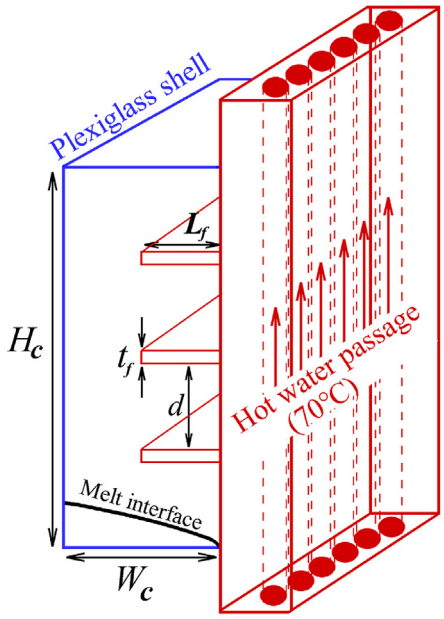

(b)

Fig. 1. Experimental rectangular storage unit (a) and its schematic drawing (b) when in contact with PCM.

storage tank. The height (H_C), depth (D_C) and width (W_C) of the tank are fixed at 120, 120 and 50 mm, respectively. Four different fin number density values with 3, 5, 7 and 9 equally-spaced fins on the heated wall and three fin lengths of 25, 35 and 45 mm were investigated, whereas the fin thickness was varied between 0.74 and 4 mm. For all of these cases, the total fin and PCM volumes remained constant at values of 36 cm^3 and 720 cm^3, respectively, providing a constant fin to PCM ratio of 5%. Table 1 lists the design parameters of the cases studied in the present work.

Lauric acid, commonly known as dodecanoic acid, with 99% purity (obtained from PanReac Chemical) was selected as the PCM. The desirable characteristics such as high latent heat of fusion, stability after numerous thermal cycling, and medium melting temperature range make dodecanoic acid a favorable PCM for medium temperature applications. Table 2 lists the thermophysical properties of the lauric acid simulated in this study [43].

3. Numerical simulation

3.1. Mathematical formulation

The enthalpy-porosity approach, proposed by Voller and Prakash [44], has been widely used to simulate the phase change process. In this method, the computational domain is considered as a porous region. The porosity value is associated with the generated liquid PCM in each cell volume, and it ranges from zero (solid PCM) to one (liquid PCM) [45,46]. The density of the fluid (liquid PCM) is considered to be constant in all terms except for the buoyancy term where the Boussinesq approximation is employed. The volume expansion of PCM and viscous dissipation term were also neglected during the phase change process. The governing equations for this laminar, incompressible, 2D and unsteady flow are:

Continuity:

$$\frac{\partial(u)}{\partial x}+\frac{\partial(v)}{\partial y}=0 \tag{1}$$

x-momentum:

$$\frac{\partial(u)}{\partial t}+\frac{\partial(uu)}{\partial x}+\frac{\partial(uv)}{\partial y}=-\frac{1}{\rho}\frac{\partial P}{\partial x}+\frac{\partial}{\partial x}\left(\nu\frac{\partial u}{\partial x}\right)+\frac{\partial}{\partial y}\left(\nu\frac{\partial u}{\partial y}\right)+g\beta(T-T_m)+\frac{1}{\rho}S_x, \tag{2}$$

y-momentum:

$$\frac{\partial(v)}{\partial t}+\frac{\partial(uv)}{\partial x}+\frac{\partial(vv)}{\partial y}=-\frac{1}{\rho}\frac{\partial P}{\partial y}+\frac{\partial}{\partial x}\left(\nu\frac{\partial v}{\partial x}\right)+\frac{\partial}{\partial y}\left(\nu\frac{\partial v}{\partial y}\right)+g\beta(T-T_m)+\frac{1}{\rho}S_y. \tag{3}$$

In these relations u and v represent the velocity components in the x- and y-directions, respectively. β is the thermal expansion coefficient, ρ denotes the density, and g is the gravitational acceleration. To take into account the impact of the phase change in the mushy region, the terms S_x and S_y known as the Darcy damping factors were added to the right-hand side of the momentum equations as:

$$S_x=-\frac{(1-\gamma)^2}{\gamma^3+\varepsilon}A_{mushy}u, \tag{4}$$

$$S_y=-\frac{(1-\gamma)^2}{\gamma^3+\varepsilon}A_{mushy}v. \tag{5}$$

Here, γ is the volume fraction of the generated liquid PCM varying from zero to one and ε takes on a negligibly small value (here 0.001) to prevent division by zero for the case of zero liquid fraction (i.e. when the entire domain is still in the solid state). The solid-liquid interface is treated as a mushy region and A_{mushy} is a mushy zone constant which controls the velocity damping within the mushy region and its numerical value is typically varied between 10^5 and 10^8 ; in the current work $A_{mushy}=5\times10^6$.

The relevant Energy relation is:

$$\frac{\partial}{\partial t}(h)+\frac{\partial}{\partial x}(uh)+\frac{\partial}{\partial y}(vh)=\frac{1}{\rho}\frac{\partial}{\partial x}\left(k\frac{\partial T}{\partial x}\right)+\frac{1}{\rho}\frac{\partial}{\partial y}\left(k\frac{\partial T}{\partial y}\right), \tag{6}$$

where h is the total enthalpy of the PCM which is computed as the sum of sensible enthalpy (h_{sens}), and latent heat (h_{lat}) as follow:

Table 1
Fin dimensions for different configurations of latent heat storage units.

Fin number	Fin length (L_f), mm	Fin thickness (t_f), mm	Fin spacing (d), mm
3	25	4	27
	35	2.86	27.85
	45	2.22	28.33
5	25	2.4	18
	35	1.71	18.57
	45	1.33	18.89
7	25	1.71	13.50
	35	1.22	13.93
	45	0.95	14.17
9	25	1.33	10.8
	35	0.95	11.14
	45	0.74	11.33

Table 2
Thermophysical properties of the lauric acid [43].

Specific heat capacity solid/liquid (kJ/kg K)	2.18/2.39
Melting temperature range (°C)	43.5/48.2
Latent heat of fusion (kJ/kg)	187.21
Thermal conductivity solid/liquid (W/m K)	0.16/0.14
Density solid/liquid (kg/ m^3)	940/885
Kinematic viscosity (m^2/s)	6.7×10^{-6}

$$h = h_{sens} + h_{lat} \tag{7}$$

$$h_{sens} = h_{ref} + C_p \int_{T_{ref}}^{T} dT \tag{8}$$

C_p is the specific heat capacity calculated at the reference temperature (T_{ref}). The stored heat is computed by summing up of the value of latent heat for each cell at each time step:

$$h_{lat} = \gamma \mathrm{l} \tag{9}$$

The liquid fraction, γ, is defined as:

$$\gamma = \begin{cases} 0 \quad if \quad T < T_{solidus}\ , \\ \dfrac{T - T_{solidus}}{T_{liquidus} - T_{solidus}} \quad if \quad T_{solidus} \le T \le T_{liquidus}, \\ 1 \quad if \quad T > T_{liquidus}. \end{cases} \tag{10}$$

A separate energy equation is solved to obtain the fin temperature, that is:

$$(\rho C_p)_{fin} \frac{\partial T}{\partial t} = k_{fin} \left[\frac{\partial^2 T}{\partial x^2} + \frac{\partial^2 T}{\partial y^2} \right] \tag{11}$$

The above-mentioned equations are discretized by implementing the finite-volume method using a staggered grid network. The SIMPLE algorithm was selected to tackle the pressure-velocity coupling. To discretize the pressure, momentum, and energy equations the PRESTO and second-order upwind schemes were employed, respectively. The under-relaxation factors of 0.2, 0.2, 0.2, 0.1, and 0.3 were chosen for the pressure correction, density, momentum, energy, and liquid fraction fields, respectively. The convergence criterion is set as 10^{-6} for continuity, velocity, and energy equations, and the maximum number of iterations in each time step is set to 200.

3.2. Boundary conditions and grid details

The adopted initial and boundary conditions are summarized as follows:

At $t = 0$, $T_{init} = 24\ ^\circ C$,

1. No-slip boundary condition on the walls, $u = v = 0$,
2. On the heated wall of the enclosure, $T = T_w = 70\ ^\circ C$,
3. For the insulated walls of the enclosure, $\frac{\partial T}{\partial x} = \frac{\partial T}{\partial y} = 0$,
4. The coupled boundary condition between the fin surfaces and PCM domain demand that $T_{fin} = T_{PCM}$, $k_{fin} \frac{\partial T_{fin}}{\partial n} = k_{PCM} \frac{\partial T_{PCM}}{\partial n}$, with n standing for the direction normal to the fin's surface.

A schematic diagram of the computational domain along with the computational grid are shown in Fig. 2(a). The generated mesh was refined at the heated solid-PCM interfaces. The results of the grid independence tests for the 3-fins vertical enclosure together with the corresponding computational time are illustrated in Fig. 2(b). At first, the time step was fixed at 0.1 s while the spatial grid size varied from 2000 to 128,000. As seen, the effect of the number of grids on the average temperature becomes minimal when the number of cells grows beyond the mesh elements of 32,000. By fixing the mesh elements to 32,000, three different time steps of 0.5, 0.1 and 0.05 s were analyzed. No considerable deviation in the average temperature is noted when the time step size is reduced from 0.1 to 0.05 s. Thus, the time step of 0.1 s and grid numbers of 32,000 with minimum and maximum edge sizes of 0.1 and 0.8 mm were selected for simulations noting the tradeoff between computational cost and numerical error. Furthermore, the effect of the mesh elements and time steps variation on the trend evolution of the melt fraction, along with the quantitative percentage error for the 3-fins vertical enclosure, is presented in Fig. 2(c).

3.3. Numerical simulation validation

The variations of the PCM temperature within the 3-fin vertical enclosure are recorded by T-type thermocouples at twenty-six different locations in the mid-section of the tested storage unit (Fig. 3(a)). The positions of the mounted thermocouples are shown in Fig. 3(b). The instantaneous average temperature of the PCM is calculated as:

$$T_{avg}(t) = \sum_{i=1}^{i=26} (T_i(t) / 26) \tag{12}$$

where $T_i\ (t)$ is the recorded instantaneous temperature at each thermocouple location.

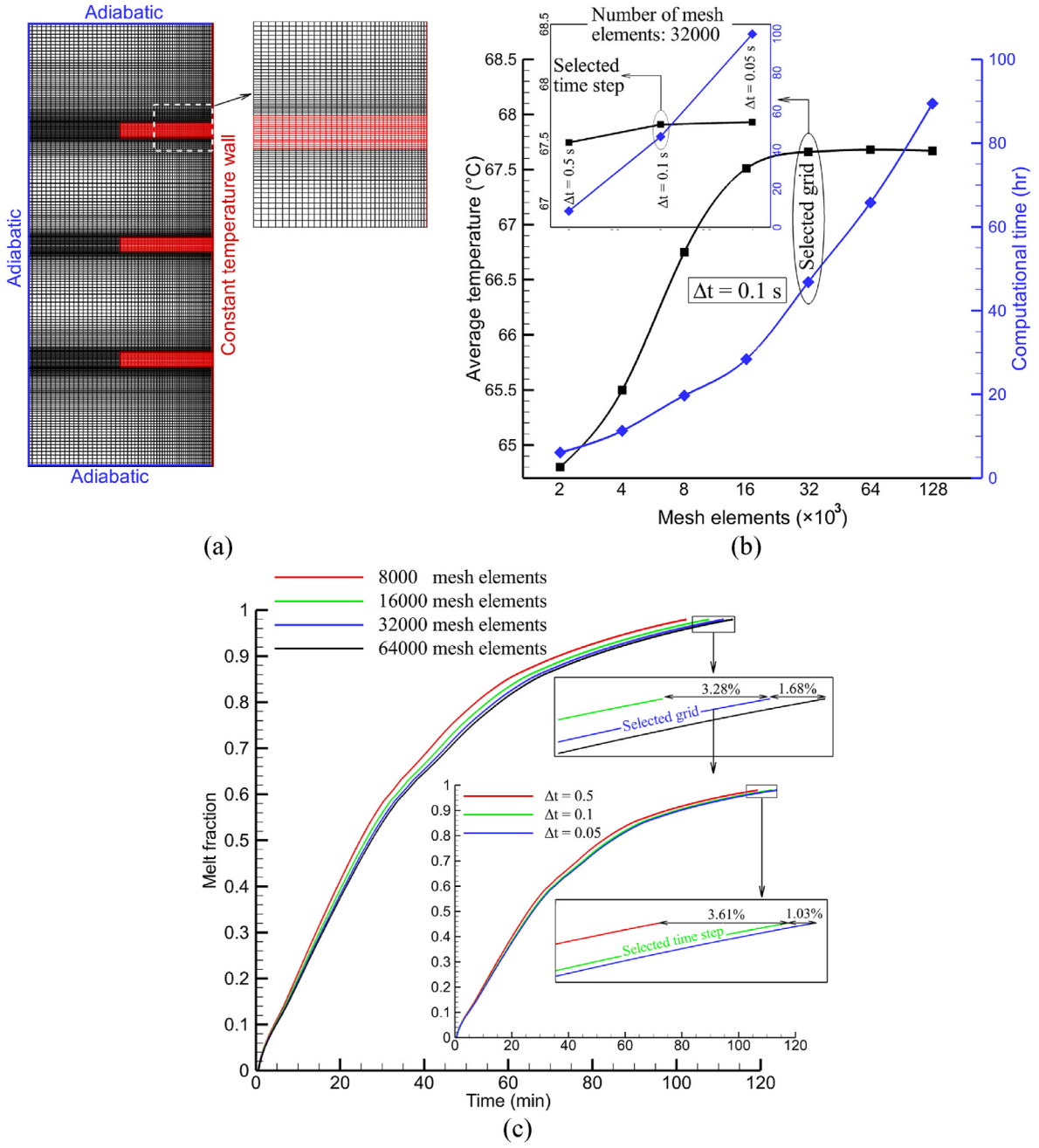

Fig. 2. (a) The employed computational mesh for the numerical simulation and (b) mesh and time independency test results (c) sensitivity analysis on the liquid fraction evolution curves.

The comparison between the numerically-computed and experimentally-measured values of the average temperature of the PCM during melting is depicted in Fig. 4. As seen, the numerical and experimental results follow similar trends and exhibit a maximum error of 6.7%. Such discrepancies between the numerical and experimental results could be attributed to:

1 The thermal properties of PCM were assumed to be temperature-independent, while they slightly varied with temperature during the experiments,
2 The uncertainty associated with the thermophysical properties measurements of PCM, including specific heat capacity, latent heat of fusion, thermal conductivity, density, and viscosity [43].

Fig. 5 compares the numerical and experimental results for the PCM's melt fraction of the 3-fin vertical enclosure case. As seen, the numerical simulation predicts a slightly faster melting rate at about 80 min of the melting process with a maximum error of 5.4% calculated at 46 min.

Fig. 6 depicts the qualitative comparison between the numerical melt fraction contours and experimental photographs captured by Kamkari and Karami [47] at four different time instants of 20, 40, 60 and 80 min. In the experimental photographs, the black and white colors represent the liquid and solid PCM, respectively, whereas in numerical contours the white and blue colors indicate the liquid and solid PCM, respectively. An excellent visual agreement with acceptable precision in the prediction of melt interface location can

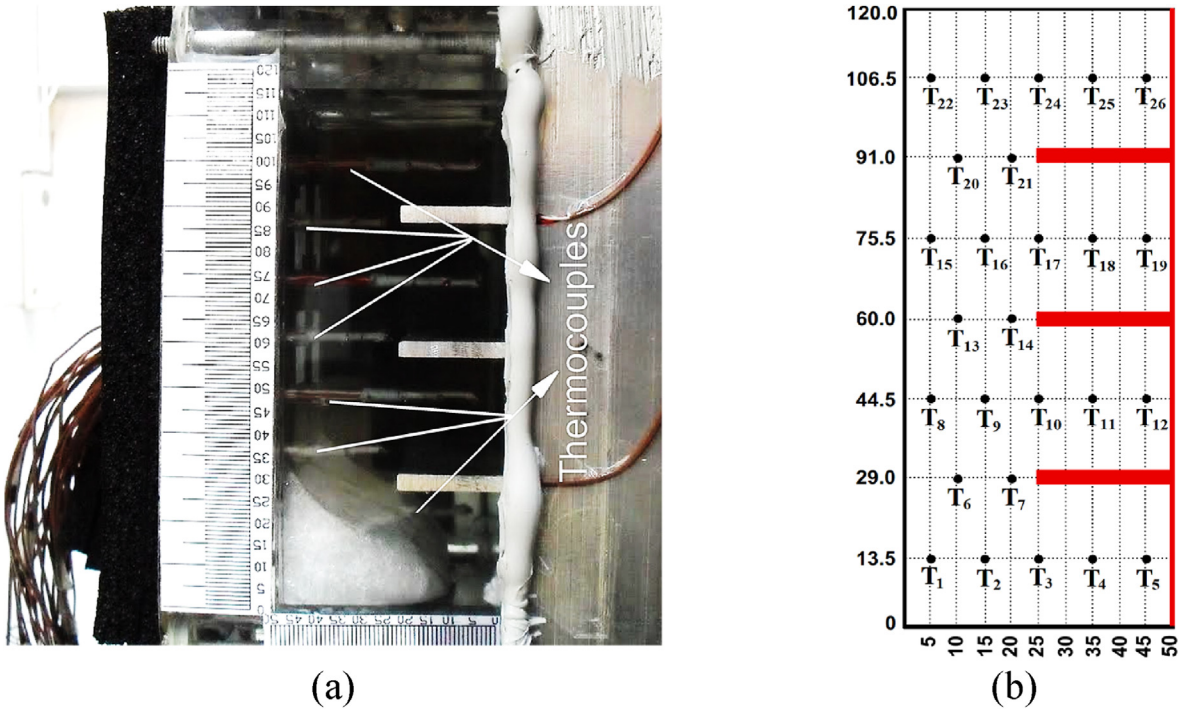

Fig. 3. (a) Photograph of the mounted thermocouples in the test unit and (b) locations of the thermocouples within the PCM.

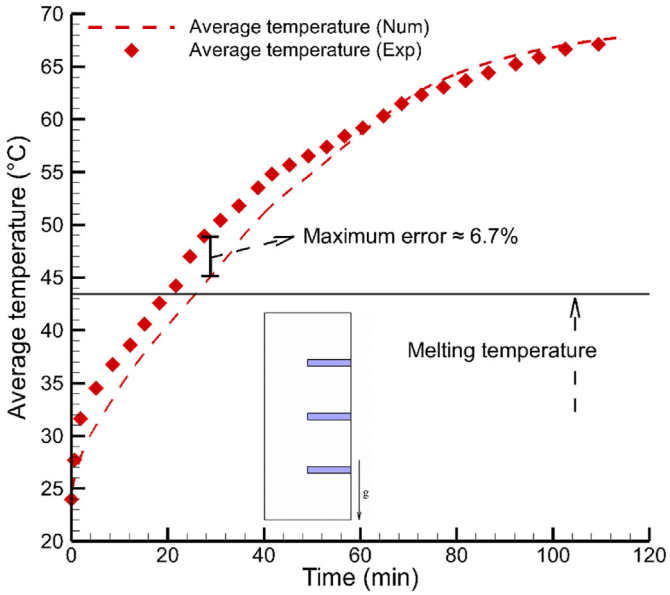

Fig. 4. Comparison of the PCM average temperature between the numerical predictions and experimental measurements during melting.

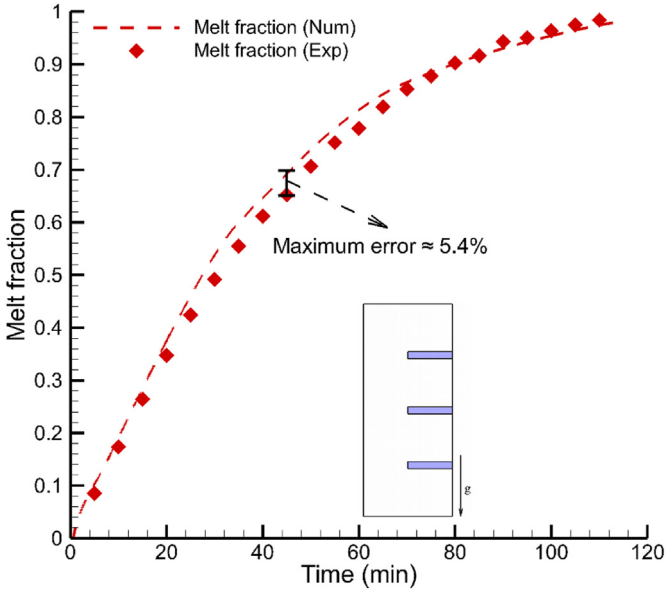

Fig. 5. Comparison between the numerical and experimental results of the melt fraction.

be observed. Moreover, the greater influence of natural convection for time instants equal and greater than 40 min is evident, whereas at the earlier time instant of 20 min, the cell-to-cell variations is minimal indicating the dominant role of thermal diffusion on the melting process.

4. Results and discussions

Figs. 7 and 8 illustrate the evolution of the melt front, temperature field, and streamlines at five different time instants for vertical and horizontal enclosures, respectively, while the fin length is varied from 25 to 45 mm. Considering the vertical enclosures (i.e. horizontal fins) at the early stage of the melting process (10 min), one notes that heat is transported predominantly by conduction giving rise to a nearly uniform melting pattern adjacent to the hot plate and fins. Also, the liquid layer thins alongside the fins indicating a temperature gradient between the fin base and tip. Hence, the liquid fraction at the fin tips for the fin length of 45 mm is lower than those of the 35 and 25 mm. The streamlines demonstrate the development of multiple small vortices (thermal plumes) above the

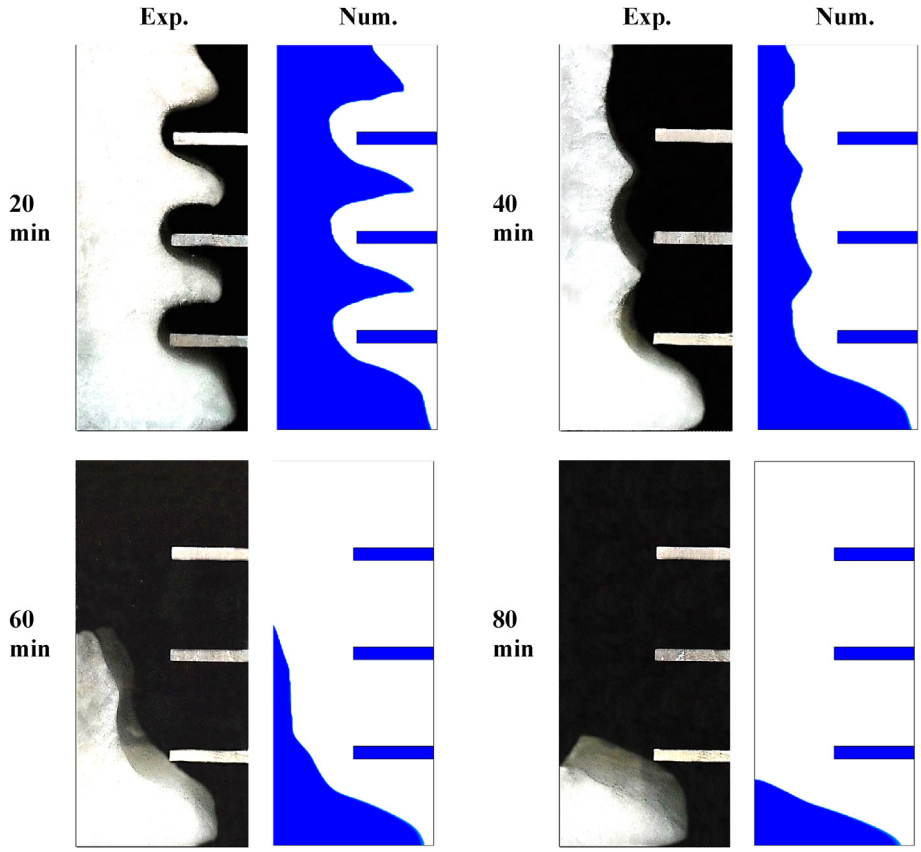

Fig. 6. The qualitative comparison of melt front propagation between experimental [47] and numerical results.

top surfaces of the fins due to the rising of locally-hot fluid and three counterclockwise rotating vortices adjacent to the vertical active hot plate. The wavy shape of the melt interface above the fins is due to the formation of such vortices within the locally unstable thermal layer, also known as the Benard cells. As time elapses more PCM is melted and buoyancy forces create natural convection flow patterns. With increasing the gap between the tip of the fins and solid PCM, the hot liquid PCM ascends upward through the gap and results in the accumulation of more molten PCM at the top part of the enclosures. According to the streamlines, at the time instant of 30 min, the small vortices merge and form four larger vortices and multiple thermal plumes. The impingement of the hot liquid PCM lumps known as thermal plumes to the solid-liquid interface causes a wavy interface. Thermal plumes rise between and above the two adjacent vortices, hit the melting interface, and reject their energy to the solid PCM, thereby the plume loses energy, gets denser and fall. The establishment of such flow pattern increases the thermal energy storage rate by direct energy transferring from the hot wall to the melting interface while enhancing the melting rate by augmenting the mixing of the liquid PCM. The temperature contours at the time instant of 30 min clearly show the formation of thermal plumes at the tip of the fins for the fin length of 25 and 35 mm, while in the enclosure with fin length of 45 mm, the thermal plumes can also be seen in the middle of the fins in addition to tip. By downward shrinking of the solid PCM, the convection currents get weaker, vortices unify, the thermal plumes subside and consequently, the melting rate decreases. The temperature contours at the final stages of the melting process clearly show the formation of thermally stratified layers at the upper part of the enclosure, which is also evident from reducing the frequency of the streamlines at the upper region of the enclosures. Henceforward, the conduction heat transfer mechanism is resumed again and will be responsible for melting the remainder of the solid PCM. Fig. 8 depicts the melting process in the horizontal enclosures (i.e. vertical fins) heated from the bottom active wall. The mounted fins are aligned with the upward flow caused by natural convection within the horizontal storage tank and this significantly improves the melting rate compared with the vertical enclosure (Fig. 7). The melt front contours show the formation of multiple concavities above the fins, which stretch as the heat transfer mechanism shifts from thermal conduction to natural convection. After 10 min, the multiple small vortices can be observed above the hot plate surface contrary to the vertical enclosures in which the vorticities were established atop the fins. Moreover, two counter-rotating vortices around each fin, regardless of the width and length of the fins can be observed. During the early stages of strengthening of the convection mechanism, the heated liquid PCM flows upwards along the fins, impinges to the melt interface, cools and descends in the gap between two adjacent fins. The temperature field contours at time instant of 20 min, display the development of two thermal plumes above the fins for enclosure with fin length of 25 mm, while for fin length of 35 and 45 mm, it reduces to one for each fin. As time goes on, the vortices join and form bigger recirculating eddies.

The transient melt fraction of the vertical and horizontal enclosures for different fin lengths along with the corresponding complete melting times are illustrated in Fig. 9. For a given fin number density, the melt fraction curves are almost indistinguishable during the conduction stage (the first 10 min). On the contrary, when convective effects kick in, different trends are observed. Results pertinent to horizontal enclosures surpass those of vertical ones with the same fin length due to the higher intensity of the convection currents. For the vertical unit cases, there is a

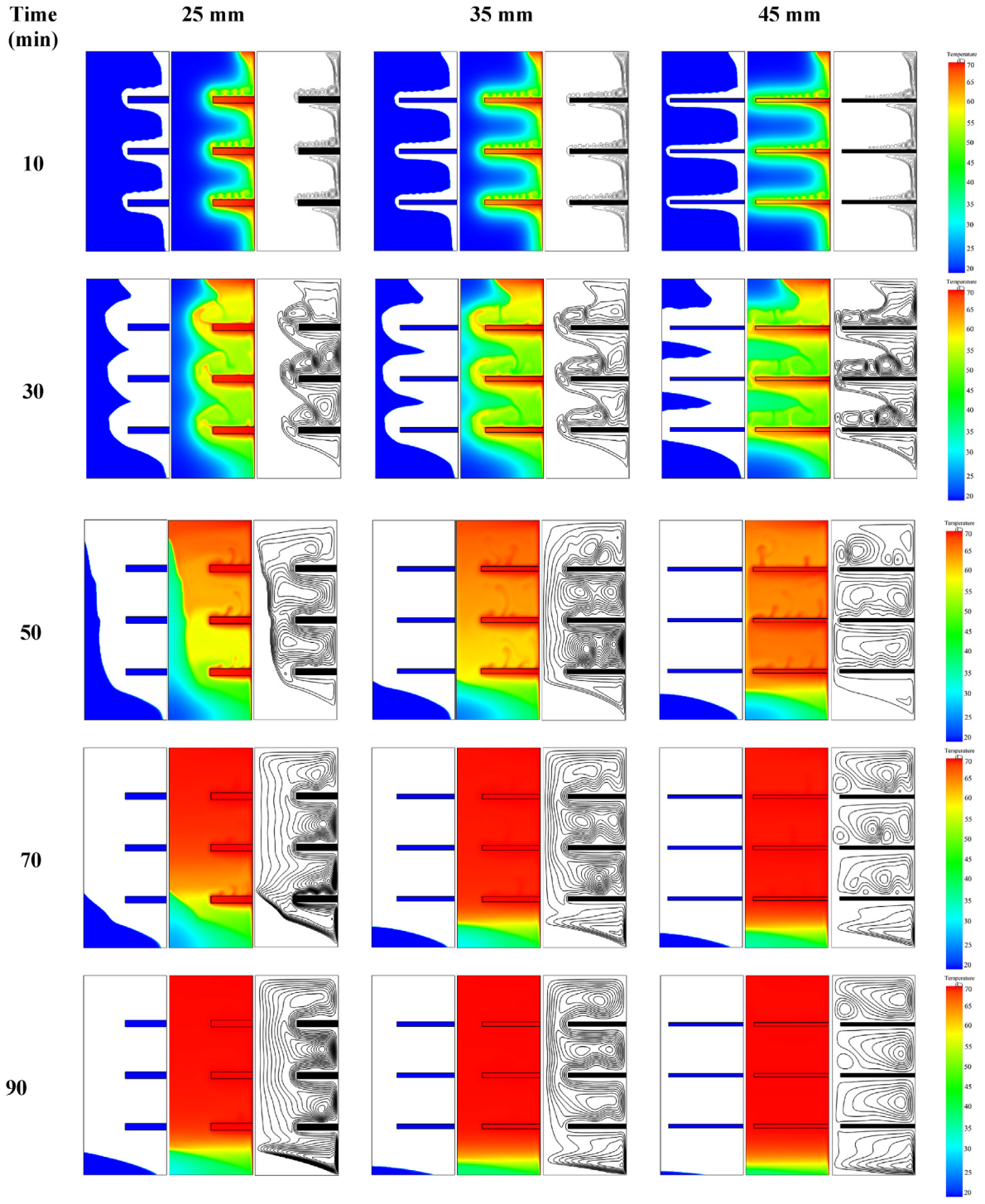

Fig. 7. Melt front, temperature field and streamlines contours for the vertical enclosures at different fin lengths.

specific melt fraction beyond which the melting rate slows down. This can be attributed to the complete melting of the confined solid PCM between the fins and the emergence of the local thermal stratification region in these pockets. Here, this threshold is termed as the shifting point. For example, the shifting point in the 5-fin enclosures with fin lengths of 25, 35, and 45 mm have occurred at melt fractions of 0.53, 0.71, and 0.87, respectively, which clearly shows that increasing the fin length delays the emergence of such shifting points. According to the complete melting time chart of the 3-fin enclosures, the shortest melting time is 44.4 min pertinent to the horizontal enclosure with a fin length of 45 mm. This shows a melting time reduction of 60.8% compared with the vertical enclosure with fin length of 25 mm as the benchmark. Examining the melting times in horizontal and vertical enclosures with equal number of fins one realizes that the shortest melting time coincides with the horizontal enclosure with the longest fins. The shortest melting time is that of a 9-fin horizontal enclosure with a fin length of 45 mm. Compared with the benchmark case, the melting process

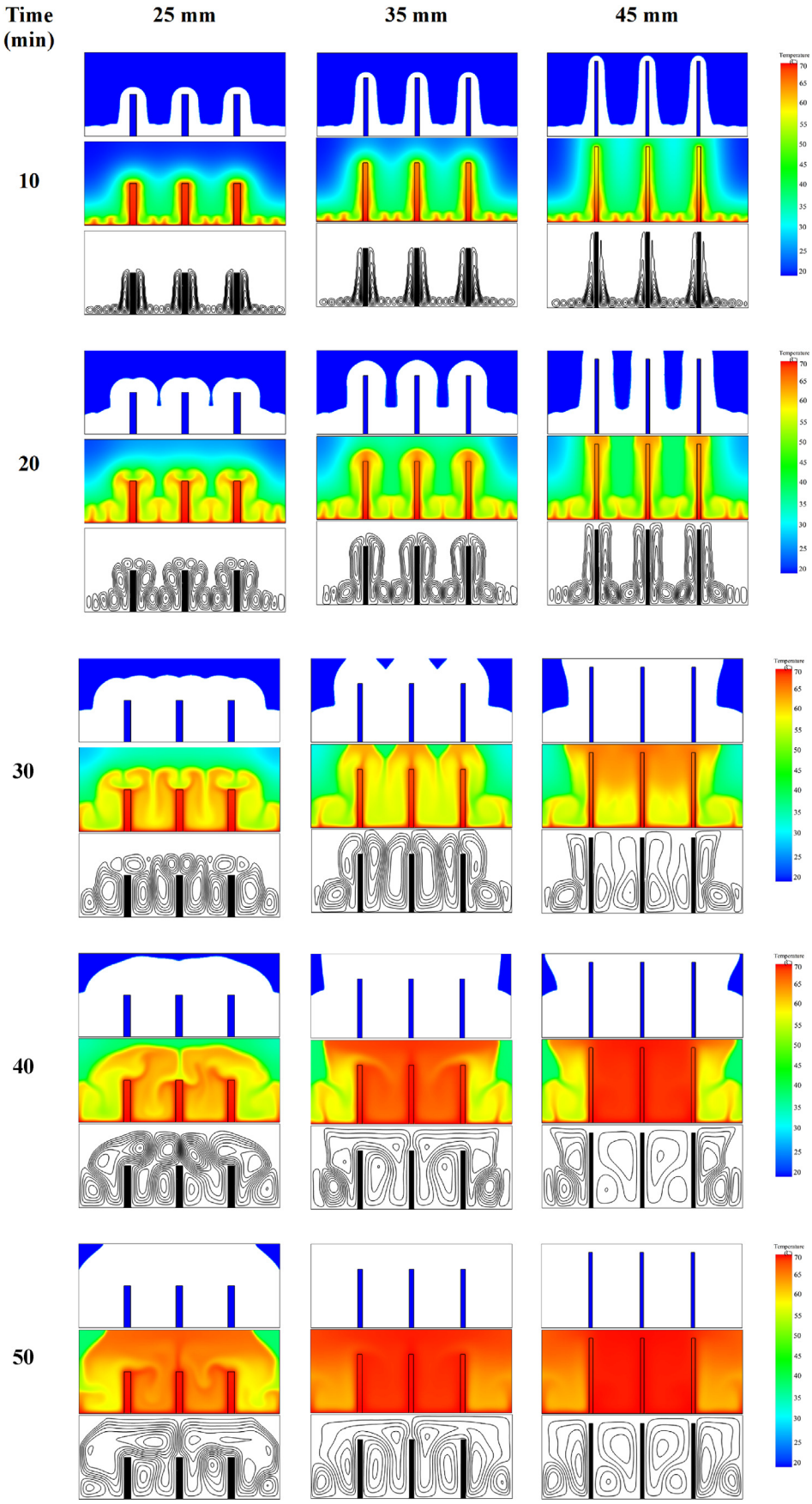

Fig. 8. Melt front, temperature field and streamlines contours for the horizontal enclosures at different fin lengths.

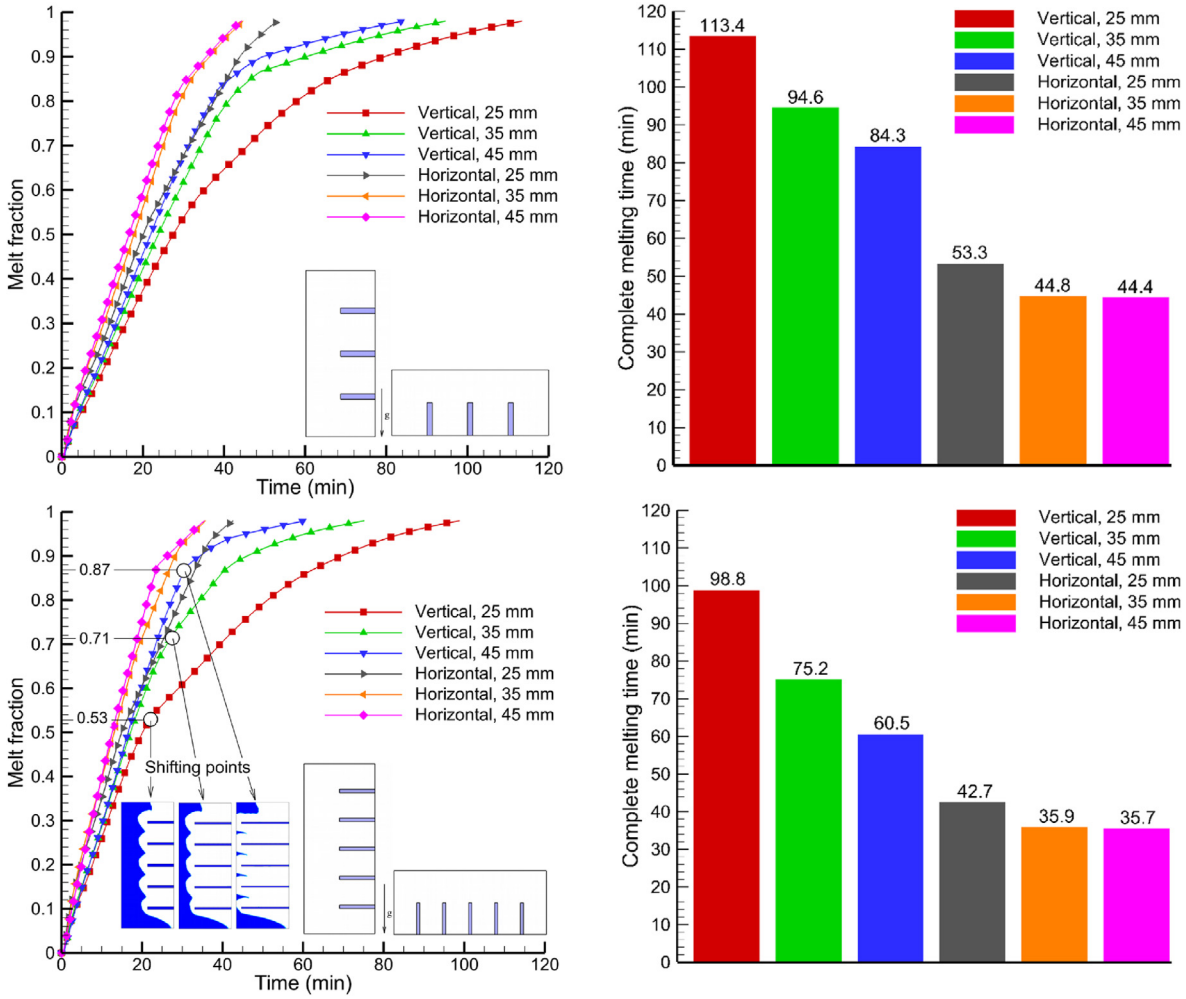

Fig. 9. The effect of the fin configurations and the number of fins on melt fraction evolution of PCM along with the corresponding melting times.

is shorter by 75.1%. It should be mentioned that for both fin lengths of 25 and 35 mm of horizontal enclosures, increasing the fin number from 7 to 9, not only does not further reduce the melting time, but also slightly prolongs the process. This can be attributed to weaker convective patterns as a result of increased fin numbers as will be explained later in this paper.

The radar chart provides useful information regarding the uniform melt fraction growth over time. Fig. 10 depicts the radar chart of the melt fraction variation during the first 50 min of the melting process for the vertical (a) and horizontal (b) enclosures. The slow growth in melt fraction is observed for the vertical cases, while the uniform increasing pattern until the end of the melting process can be observed for the horizontal cases. It is worth noting that the solid-liquid interface acts as a cold surface (heat sink) for driving the convection currents. In horizontal enclosures, the length of the interface is almost constant throughout the process, while in vertical cases the interface shrinks during the melting process. Hence, a sluggish trend in vertically-oriented enclosures can be attributed to the weakening of convection flow and resumption of a slow conduction mechanism at the final stages of the melting process.

The transient melting enhancement ratio is another quantitative parameter that can be employed to evaluate the melting behavior within the enclosures. In this study, the melting enhancement ratio (MER) is defined as:

$$MER = \frac{lf_{(t)} - lf_{(t)}(Base\ case)}{lf_{(t)}(Base\ case)} \tag{13}$$

in which $lf_{(t)}$ is the transient melt fraction of the specific case. For both vertical and horizontal enclosures, the 3-fin enclosure with fin length of 25 mm is taken as a base case for comparison. Fig. 11 shows the variation of *MER* for vertical (a) and horizontal (b) enclosures. For all case studies, the enhancement ratio increases steeply till it reaches a peak and then gradually decreases. Increasing the fin numbers results in higher values of enhancement ratio, and with time elapsing, the difference in MER values becomes less pronounced in both vertical and horizontal enclosures. For 7-fin and 9-fin vertical and horizontal enclosures with fin lengths of 25 mm, the sharper decline compared to other cases can be observed after the attained peak time. For example, after about 20 min of the melting process, the 5-fin vertical enclosure with fin length of 45 mm performs better than the 9-fin unit with fin length of 25 mm. Therefore, using longer fins at lower number density can be more effective than using lower fins at higher number density.

In order to classify the heat transfer mechanisms governing the melting process, the transient surface-averaged Nusselt number

($\overline{Nu}$) is calculated as follows:

$$\overline{Nu} = \frac{\overline{h}_{(t)} H}{k_l}, \tag{14}$$

where $\overline{h}_{(t)}$ represents the surface-averaged heat transfer coefficient and is calculated through the following equation:

$$\overline{h}_t = \frac{Q_{(total)}(t)}{A_w (T_w - T_m)\Delta t} \tag{15}$$

By substituting $\overline{h}_{(t)}$ from equation (15) into (14), $\overline{Nu}$ can be calculated through the following equation:

$$\overline{Nu} = \frac{Q_{(total)}(t).H}{A_w (T_w - T_m)\Delta t.k_l}, \tag{16}$$

where $Q_{(total)}(t)$ is the total absorbed heat (latent and sensible) by the lauric acid during the time interval of δt and H represents the characteristic length which is considered as the height of the vertical enclosure (H_c). Also, T_w is the wall temperature (70 °C) and T_m denotes the melting temperature, which is selected as an arithmetic mean of the upper and lower melting temperature range ($\frac{43.5+48.2}{2} = 45.58$ °C). A_w is defined as the total heat transfer area considering the heated wall and fin surface areas:

$$A_w = (D_c \times H_c) + 2N\left(L_f \times D_c\right), \tag{17}$$

where D_c and H_c are the depth and height of the enclosure, respectively. Here, N and L_f represent the number and length of the fins, respectively (Table 1). Fig. 12 presents the transient variation of $\overline{Nu}$ for different fin configurations within the vertical (a) and horizontal (b) enclosures, respectively. For all fin configurations, the $\overline{Nu}$ starts with relatively high values, resulting from the low thermal resistance of the thin layer of melted PCM during the close-contact-melting stage. As the melted layer progresses, the thermal resistance between the heat transfer surface and solid-liquid interface increases that leads to a sharp decline in $\overline{Nu}$. With higher liquid fraction and initiation of convection, the sharp decreasing trend is ceased for both vertical and horizontal enclosure. From this moment forth, the very gentle decreasing trend in $\overline{Nu}$ values can be seen for both vertical and horizontal enclosures with the difference that the decreasing slope is milder in the horizontal cases than in the vertical ones. Such variation trend in horizontal enclosures clearly shows the development of stronger natural convection currents when compared to vertical enclosures. Interestingly, for both vertical and horizontal LHSU, the superiority of the enclosures with the higher number of fins diminishes sooner than those with lower numbers. The hindering effect of the fins against the upward convection currents is responsible for such behavior.

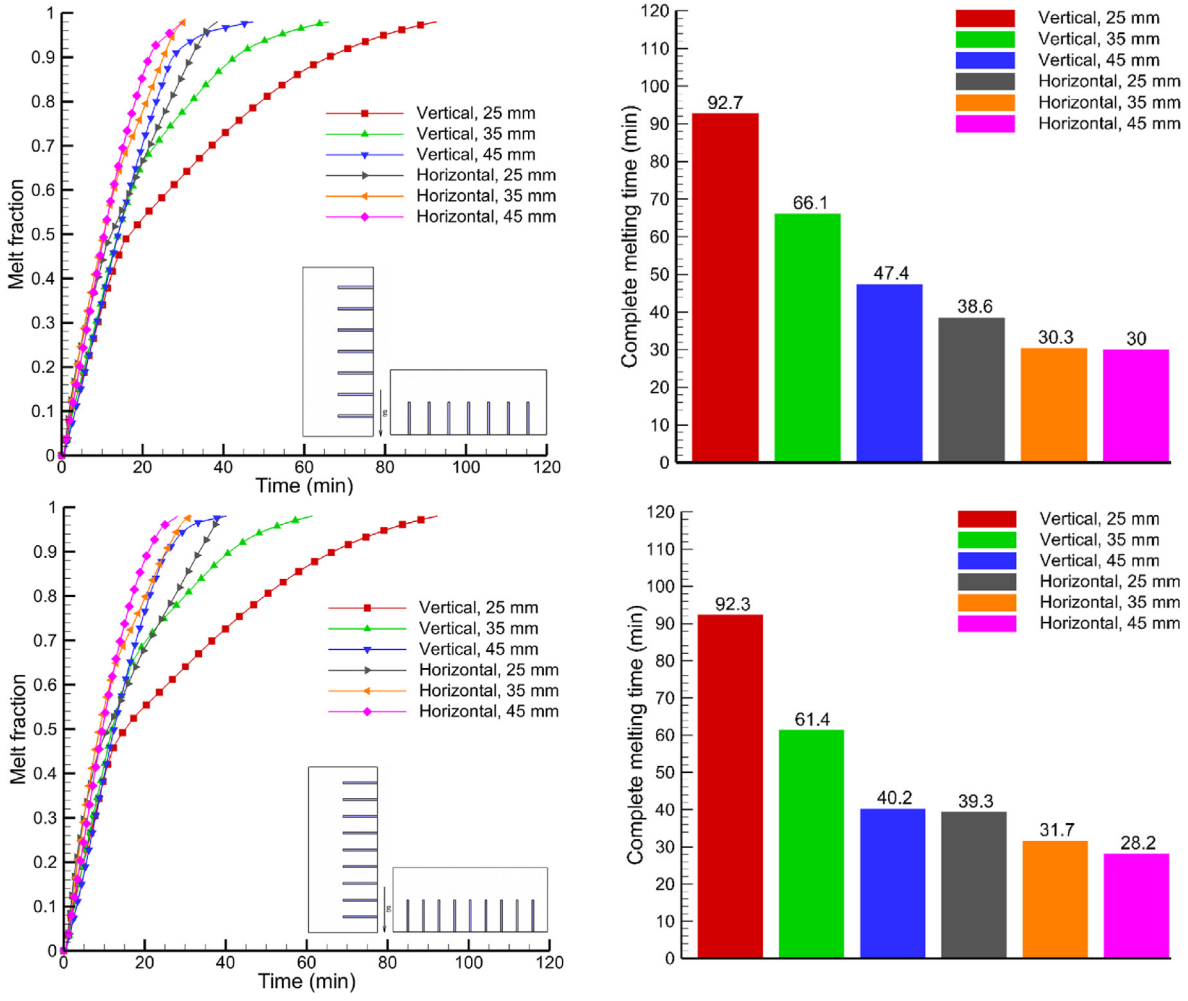

Fig. 9. (*continued*).

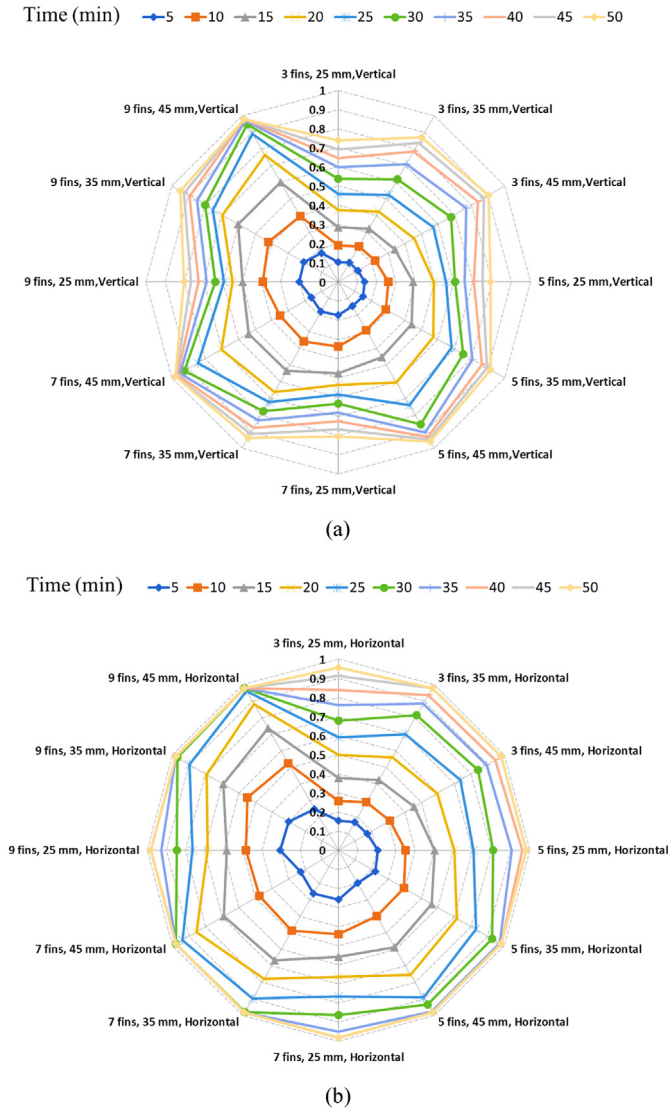

Fig. 10. The radar chart of the melt fraction variation for (a) vertical and (b) horizontal enclosures.

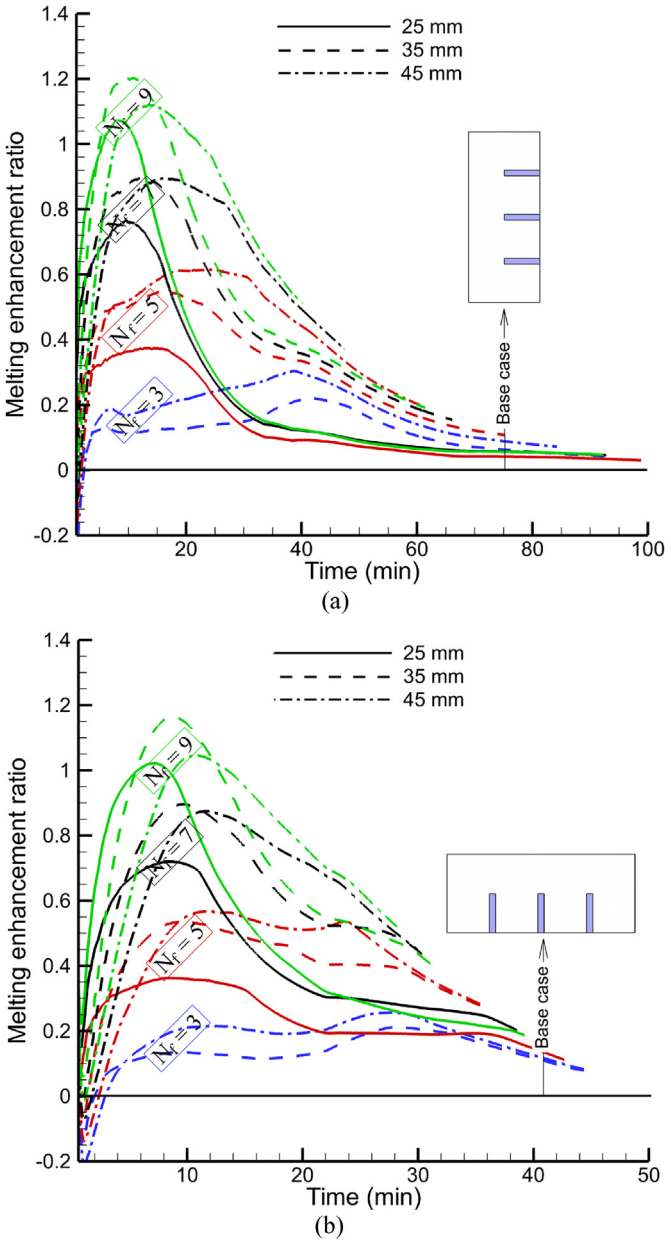

Fig. 11. The transient variation of melting enhancement ratio for (a) vertical and (b) horizontal enclosures.

To further examine the impact of the number of fins on the intensity of convection flows, Fig. 13 illustrates the variations of average velocity within the vertical (a) and horizontal (b) enclosures with melt fraction for the fin length fixed at 25 mm. It can be observed that the average velocity rises, reaches its maximum value, and then decays, which indicates depression of convection flows. The peak times in these graphs represent the instant the melting interface reaches the opposite wall and starts shrinking. Considering the two cases with the same fin configuration but different enclosure orientations, it can be seen that the decline in the average velocity takes place at higher values of liquid fraction in horizontal enclosures than the vertical ones. This suggests that the enclosures heated from the bottom take advantage of the development of convection currents until near the end of the melting process, while convection flows diminish earlier in vertical enclosures. Also, the peak value of average velocity increases by employing the horizontal enclosure. For example, the liquid fractions correspond to the peaks of the maximum velocities for 3-fin vertical and horizontal enclosures are 5.12 mm/s and 7.03 mm/s, respectively; revealing the development of more powerful convection currents in horizontal enclosures. Moreover, the average velocity increases by reducing the fin numbers indicating that the strength of convection flows is enhancing as the number of fins decreases. It can also be seen that the oscillations in average velocity curves diminish with increasing the number of fins implying that the strength of the natural convection in the liquid PCM and consequently the number of the small vortices reduces as the number of fins increases.

For a more comprehensive understanding of the problem, the time-averaged heat transfer rate ($< \overline{Q} >$) and the time-averaged Nusselt number ($<\overline{Nu}>$) are calculated as:

$$\langle \overline{Q} \rangle = \frac{1}{t_{total}} \int_0^t \overline{Q}(t) dt, \tag{18}$$

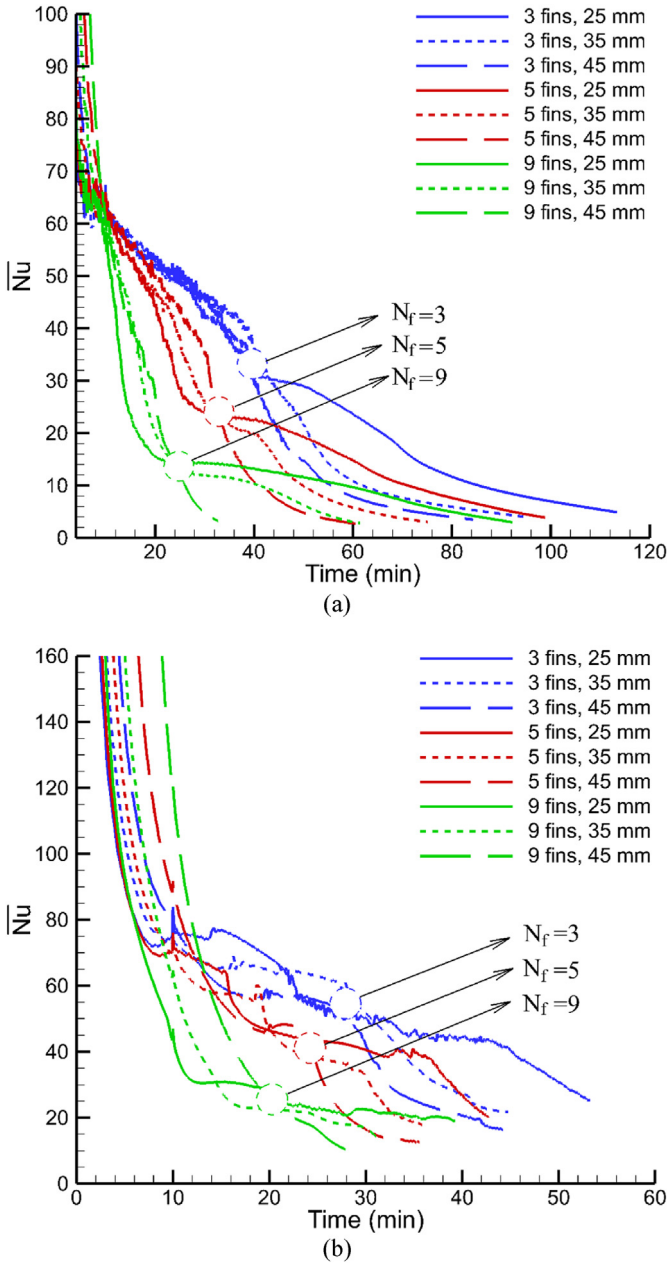

Fig. 12. The transient variation of $\overline{Nu}$ values for (a) vertical and (b) horizontal enclosures.

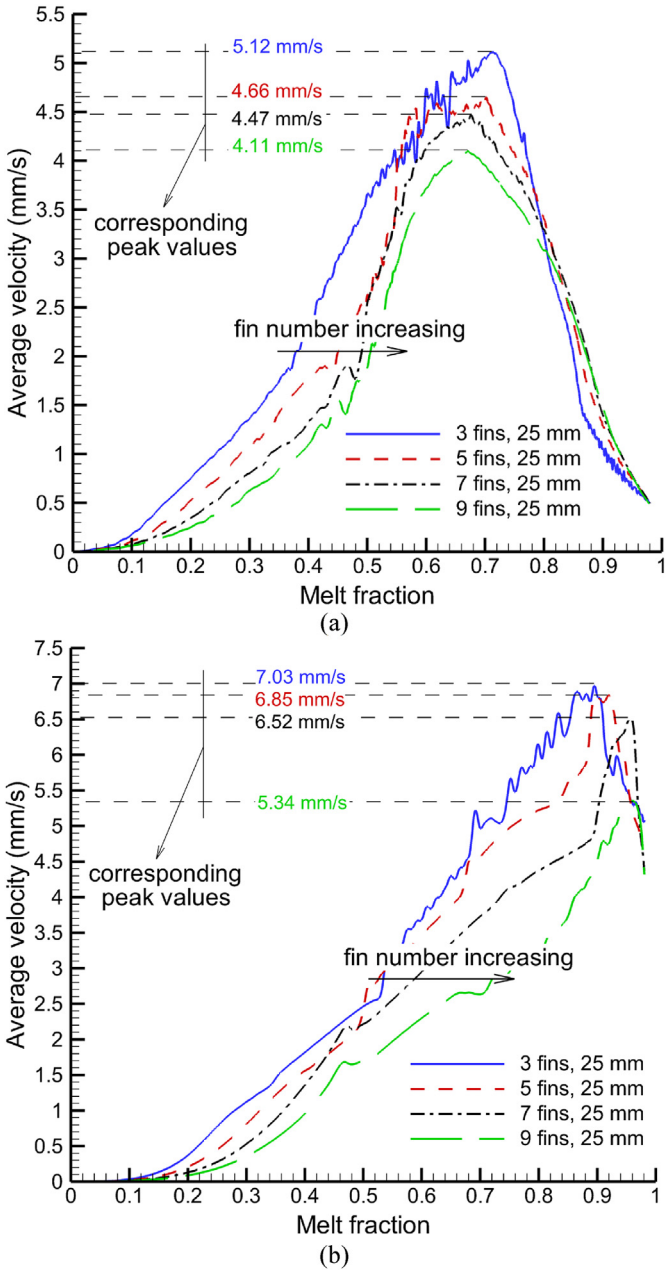

Fig. 13. Comparison of time histories of the average velocities for (a) vertical and (b) horizontal enclosures.

$$\langle \overline{Nu} \rangle = \frac{1}{t_{total}} \int_0^t \overline{Nu}(t)dt, \tag{19}$$

where $\overline{Q}(t)$ and $\overline{Nu}(t)$ are the instantaneous surface-averaged heat transfer rate and surface-averaged Nusselt number, respectively. Fig. 14 presents the variation of the time-averaged heat transfer rate and time-averaged Nusselt number with fin numbers for vertical (a) and horizontal (b) enclosures. For vertical enclosure cases, increasing the number and length of the fins results in a decrease and increase in $< \overline{Nu} >$ and $<\overline{Q}>$ values, respectively. The same decremental trend in $< \overline{Nu} >$ values of the horizontal enclosures can also be observed. The variation of $< \overline{Q} >$ in the horizontal enclosure cases for fin lengths of 25 and 35 mm indicates that increasing the fin number beyond seven reduces the heat transfer rate. In fact, in a trade-off between two essential factors of increasing the heat transfer area and decreasing the Nusselt number, the latter outweighs leading to a decrease in heat transfer rate. Interestingly, for a fin length of 45 mm, the tradeoff between the mentioned factors is weighted in favor of the first parameter which results in a slight increase in the time-averaged heat transfer rate.

Fig. 15 (a) and (b) illustrate the alteration of the stored thermal energy for vertical and horizontal enclosure, respectively. The stored thermal energy within the enclosures is comprised of two forms of sensible and latent heat. The amount of the stored latent heat is only a function of the mass of the enclosed PCM within the storage units. Since the fins volume for all the studied cases is kept constant, the amount of the latent heat for all enclosures is identical. The latent heat changes proportionately with the amount of

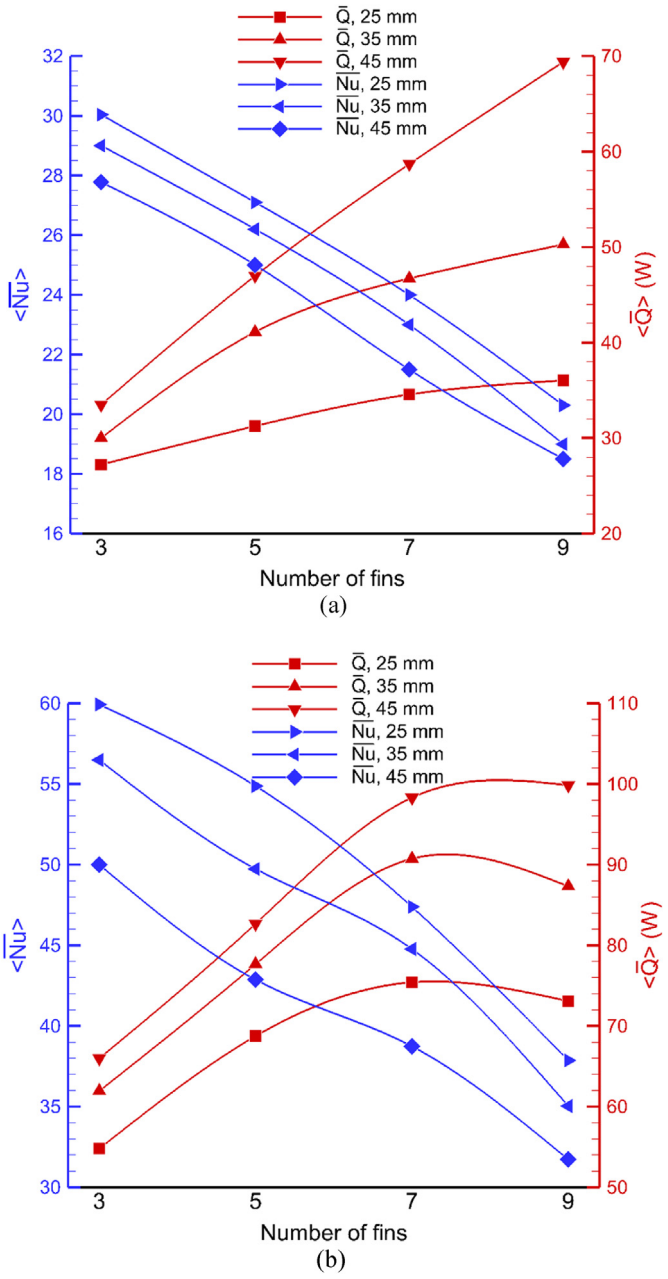

Fig. 14. Variation of the time-averaged heat transfer rate and the time-averaged Nusselt number for (a) vertical and (b) horizontal enclosures.

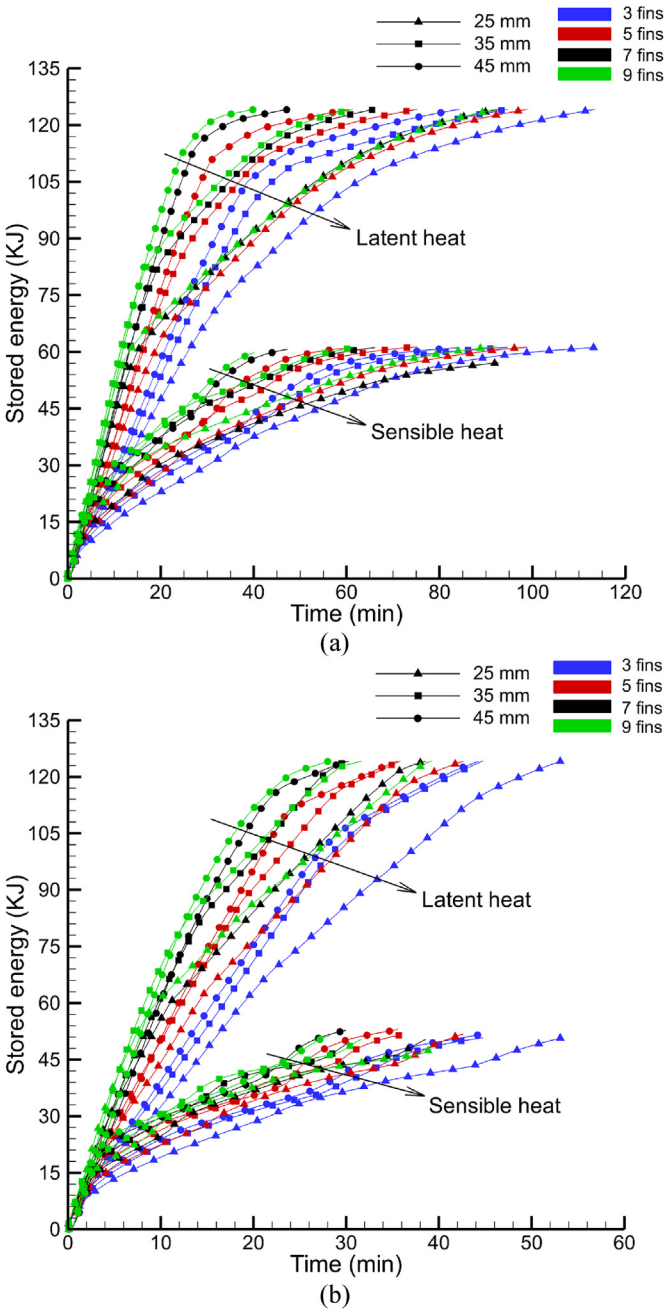

Fig. 15. Variation of the category of the stored thermal energy for (a) vertical and (b) horizontal enclosures.

melted PCM, hence the similar trends between the latent heat and melt fraction in Fig. 9 are observed. The thermally stratified region in the vertical enclosures causes a slower storage of sensible heat compared with the horizontal enclosure cases.

Fig. 16 indicates the total (final) amount of stored heat and the average PCM temperature for all cases considered here. The values of stored energy, mainly sensible form of heat, change with the average temperature. Obviously, the PCM within the vertical enclosures reaches higher average temperature compared with the horizontal ones. Horizontal enclosures can store about the same amount of heat at relatively lower temperature and shorter time compared with vertical ones. This can be beneficial for the application of PCM in thermal management of the batteries and electronics cooling where the temperature control of the device is crucial.

5. Conclusions

In the present research, the melting behavior of the lauric acid as a PCM in one-side heated vertical and horizontal rectangular thermal storage units with different fin configurations was numerically studied. The transient numerical simulations using the enthalpy-porosity approach based on the finite-volume method were performed. An excellent quantitative and qualitative agreement between the numerical and experimental results was achieved. Four fin numbers of 3, 5, 7, and 9, with different lengths of 25, 35, and 45 mm were investigated while the overall fin volume had been kept fixed. The main conclusions of this research are summarized as follow:

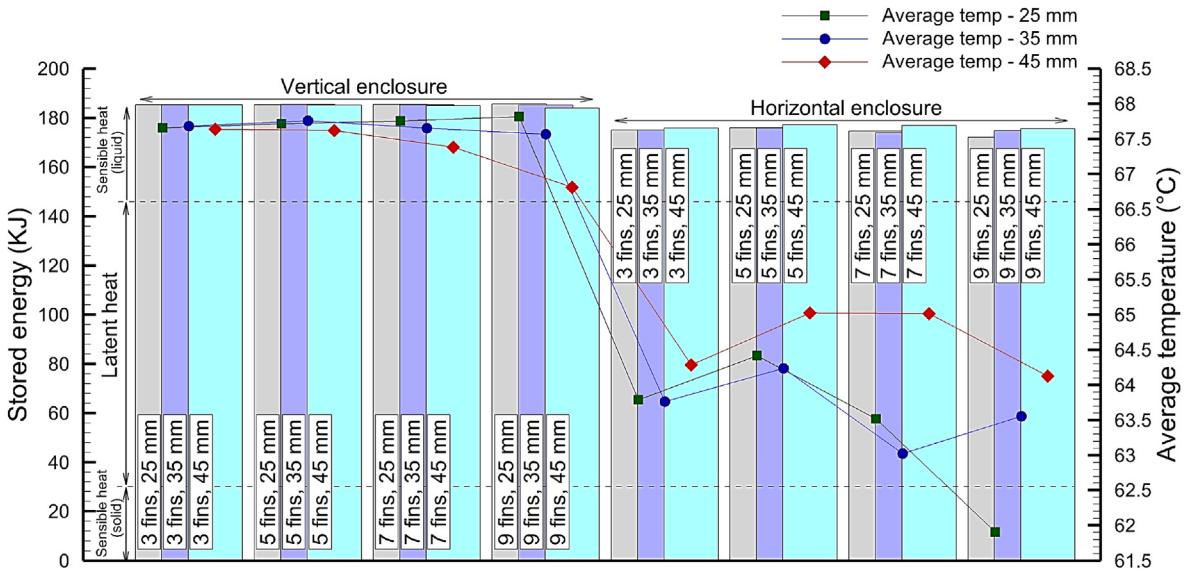

Fig. 16. Comparison of the category of stored energy and average temperature of PCM for the studied configurations.

- Mounting the fins to coincide with the direction of the upward natural convection currents can significantly improve the heat transfer rate, which results in a higher melting time reduction in the horizontal thermal storage units than the vertical ones.
- In an enclosure with a fixed number of fins, increasing the fin length improves the melting rate due to providing a higher surface area and boosting the thermal penetration depth.
- The maximum melting time reduction compared with the benchmark is 75.1%, which is exhibited by the 9-fin horizontal enclosure with a fin length of 45 mm.
- Examining the time history of the average velocities indicates that the horizontal enclosures take advantage of the development of convection currents until near the end of the melting process, whereas in vertical units the strength of the convection currents is diminished earlier due to the melt interface shrinkage.
- The decremental trend of the surface-averaged *Nu* number with increasing the fin number reveals that the strength of convection flows can be enhanced by reducing the number of fins. Also, it was concluded that the heat transfer rate is controlled by the trade-off between the increase in the heat transfer area and the decrease in the Nusselt number (hampering effect of the fins).
- The horizontal enclosures can store about the same amount of thermal energy at a relatively lower temperature and shorter melting time than the vertical enclosures, making them more applicable in temperature management sectors.

Credit author statement

Vahid Safari: Investigation, Software, Validation, Writing – original draft, Visualization, **Babak Kamkari**: Supervision, Conceptualization, Methodology, Writing, Writing – review & editing, **Kamel Hoomn**: Methodology, Writing – review & editing, **J. M. Khodadadi**: Methodology, Writing – review & editing.

Declaration of competing interest

The authors declare that they have no known competing financial interests or personal relationships that could have appeared to influence the work reported in this paper.

References

[1] Khudhair AM, Farid MM. A review on energy conservation in building applications with thermal storage by latent heat using phase change materials. Energy Convers Manag 2004;45:263–75. https://doi.org/10.1016/S0196-8904(03)00131-6.
[2] Zalba B. Review on thermal energy storage with phase change: materials, heat transfer analysis and applications. Appl Therm Eng 2003;23:251–83. https://doi.org/10.1016/S1359-4311(02)00192-8.
[3] Fu Z, Li Y, Liang X, Lou S, Qiu Z, Cheng Z, Zhu Q. Experimental investigation on the enhanced performance of a solar PVT system using micro-encapsulated PCMs. Energy 2021;228:120509. https://doi.org/10.1016/J.ENERGY.2021.120509.
[4] Atalay H, Cankurtaran E. Energy, exergy, exergoeconomic and exergo-environmental analyses of a large scale solar dryer with PCM energy storage medium. Energy 2021;216:119221. https://doi.org/10.1016/J.ENERGY.2020.119221.
[5] Huang H, Wang H, Gu J, Wu Y. High-dimensional model representation-based global sensitivity analysis and the design of a novel thermal management system for lithium-ion batteries. Energy Convers Manag 2019;190:54–72. https://doi.org/10.1016/j.enconman.2019.04.013.
[6] Yang M, Wang H, Shuai W, Deng X. Thermal optimization of a kirigami-patterned wearable lithium-ion battery based on a novel design of composite phase change material. Appl Therm Eng 2019;161:114141. https://doi.org/10.1016/j.applthermaleng.2019.114141.
[7] Adilkhanova I, Memon SA, Kim J, Sheriyev A. A novel approach to investigate the thermal comfort of the lightweight relocatable building integrated with PCM in different climates of Kazakhstan during summertime. Energy 2021;217:119390. https://doi.org/10.1016/J.ENERGY.2020.119390.
[8] Kabdrakhmanova M, Memon SA, Saurbayeva A. Implementation of the panel data regression analysis in PCM integrated buildings located in a humid subtropical climate. Energy 2021;237:121651. https://doi.org/10.1016/J.ENERGY.2021.121651.
[9] Cheng X, Zhai X. Thermal performance analysis of a cascaded cold storage unit using multiple PCMs. Energy 2018;143:448–57. https://doi.org/10.1016/J.ENERGY.2017.11.009.
[10] Al-Shannaq R, Young B, Farid M. Cold energy storage in a packed bed of novel graphite/PCM composite spheres. Energy 2019;171:296–305. https://doi.org/10.1016/J.ENERGY.2019.01.024.
[11] Mao Q, Li Y, Chen M. Design and investigation of single tank phase change thermal storage domestic hot water system. Case Stud Therm Eng 2021;25:100903. https://doi.org/10.1016/J.CSITE.2021.100903.
[12] Carmona M, Rincón A, Gulfo L. Energy and exergy model with parametric study of a hot water storage tank with PCM for domestic applications and experimental validation for multiple operational scenarios. Energy Convers Manag 2020;222:113189. https://doi.org/10.1016/J.ENCONMAN.2020.113189.
[13] Zhou Y, Zheng S, Zhang G. Study on the energy performance enhancement of a new PCMs integrated hybrid system with the active cooling and hybrid ventilations. Energy 2019;179:111–28. https://doi.org/10.1016/J.ENERGY.2019.04.173.
[14] Li XY, Yang L, Wang XL, Miao XY, Yao Y, Qiang QQ. Investigation on the charging process of a multi-PCM latent heat thermal energy storage unit for

use in conventional air-conditioning systems. Energy 2018;150:591–600. https://doi.org/10.1016/J.ENERGY.2018.02.107.
[15] Alehosseini E, Jafari SM. Micro/nano-encapsulated phase change materials (PCMs) as emerging materials for the food industry. Trends Food Sci Technol 2019;91:116–28. https://doi.org/10.1016/J.TIFS.2019.07.003.
[16] Leungtongkum T, Flick D, Hoang HM, Steven D, Delahaye A, Laguerre O. Insulated box and refrigerated equipment with PCM for food preservation: state of the art. J Food Eng 2022;317:110874. https://doi.org/10.1016/J.JFOODENG.2021.110874.
[17] Fan L, Khodadadi JM. Thermal conductivity enhancement of phase change materials for thermal energy storage: a review. Renew Sustain Energy Rev 2011;15:24–46. https://doi.org/10.1016/j.rser.2010.08.007.
[18] Zhao C, Opolot M, Liu M, Bruno F, Mancin S, Hooman K. Phase change behaviour study of PCM tanks partially filled with graphite foam. Appl Therm Eng 2021;196:117313. https://doi.org/10.1016/J.APPLTHERMALENG.2021.117313.
[19] Zhao C, Opolot M, Liu M, Bruno F, Mancin S, Flewell-Smith R, Hooman K. Simulations of melting performance enhancement for a PCM embedded in metal periodic structures. Int J Heat Mass Tran 2021;168:120853. https://doi.org/10.1016/j.ijheatmasstransfer.2020.120853.
[20] Hashem Zadeh SM, Mehryan SAM, Ghalambaz M, Ghodrat M, Young J, Chamkha A. Hybrid thermal performance enhancement of a circular latent heat storage system by utilizing partially filled copper foam and Cu/GO nano-additives. Energy 2020;213:118761. https://doi.org/10.1016/J.ENERGY.2020.118761.
[21] Rostami S, Afrand M, Shahsavar A, Sheikholeslami M, Kalbasi R, Aghakhani S, Shadloo MS, Oztop HF. A review of melting and freezing processes of PCM/nano-PCM and their application in energy storage. Energy 2020;211:118698. https://doi.org/10.1016/J.ENERGY.2020.118698.
[22] Tiari S, Hockins A. An experimental study on the effect of annular and radial fins on thermal performance of a latent heat thermal energy storage unit. J Energy Storage 2021;44:103541. https://doi.org/10.1016/J.EST.2021.103541.
[23] Kamkari B, Darvishvand L. Heat transfer augmentation of latent heat thermal storage systems employing extended surfaces and heat pipes. In: Solid–liquid therm. Energy storage. Boca Raton: CRC Press; 2022. p. 145–68. https://doi.org/10.1201/9781003213260-7.
[24] Li E, Zhou Z, Wang H, Cai K. A global sensitivity analysis-assisted sequential optimization tool for plant-fin heat sink design. Eng Comput (Swansea, Wales) 2020;37:591–614. https://doi.org/10.1108/EC-12-2018-0590.
[25] Dhaidan NS, Khodadadi JM. Melting and convection of phase change materials in different shape containers: a review. Renew Sustain Energy Rev 2015;43:449–77. https://doi.org/10.1016/j.rser.2014.11.017.
[26] Qin H, Wang Z, Heng W, Liu Z, Li P. Numerical study of melting and heat transfer of PCM in a rectangular cavity with bilateral flow boundary conditions. Case Stud Therm Eng 2021;27:101183. https://doi.org/10.1016/J.CSITE.2021.101183.
[27] Shafiq MS, Khan MM, Irfan M. Performance enhancement of double-wall-heated rectangular latent thermal energy storage unit through effective design of fins. Case Stud Therm Eng 2021;27:101339. https://doi.org/10.1016/J.CSITE.2021.101339.
[28] Cao X, Yuan Y, Xiang B, Highlight F. Effect of natural convection on melting performance of eccentric horizontal shell and tube latent heat storage unit. Sustain Cities Soc 2018;38:571–81. https://doi.org/10.1016/j.scs.2018.01.025.
[29] Seddegh S, Wang X, Mastani M, Haghighat F. Investigation of the effect of geometric and operating parameters on thermal behavior of vertical shell-and-tube latent heat energy storage systems. Energy 2017;137:69–82. https://doi.org/10.1016/j.energy.2017.07.014.
[30] Hosseinizadeh SF, Rabienataj Darzi AA, Tan FL, Khodadadi JM. Unconstrained melting inside a sphere. Int J Therm Sci 2013;63:55–64. https://doi.org/10.1016/j.ijthermalsci.2012.07.012.
[31] Tan FL, Hosseinizadeh SF, Khodadadi JM, Fan L. Experimental and computational study of constrained melting of phase change materials (PCM) inside a spherical capsule. Int J Heat Mass Tran 2009;52:3464–72. https://doi.org/10.1016/j.ijheatmasstransfer.2009.02.043.
[32] Sahoo SK, Das MK, Rath P. Application of TCE-PCM based heat sinks for cooling of electronic components: a review. Renew Sustain Energy Rev 2016;59:550–82. https://doi.org/10.1016/J.RSER.2015.12.238.
[33] Srikanth R, Nemani P, Balaji C. Multi-objective geometric optimization of a {PCM} based matrix type composite heat sink. Appl Energy 2015;156:703–14. https://doi.org/10.1016/j.apenergy.2015.07.046.
[34] Abdi A, Martin V, Chiu JNW. Numerical investigation of melting in a cavity with vertically oriented fins. Appl Energy 2019;235:1027–40. https://doi.org/10.1016/j.apenergy.2018.11.025.
[35] Nakhchi ME, Esfahani JA. Improving the melting performance of PCM thermal energy storage with novel stepped fins. J Energy Storage 2020;30:101424. https://doi.org/10.1016/j.est.2020.101424.
[36] Kalbasi R, Afrand M, Alsarraf J, Tran MD. Studies on optimum fins number in PCM-based heat sinks. Energy 2019;171:1088–99. https://doi.org/10.1016/J.ENERGY.2019.01.070.
[37] Kamkari B, Shokouhmand H. Experimental investigation of phase change material melting in rectangular enclosures with horizontal partial fins. Int J Heat Mass Tran 2014;78:839–51. https://doi.org/10.1016/j.ijheatmasstransfer.2014.07.056.
[38] Ji C, Qin Z, Low Z, Dubey S, Choo FH, Duan F. Non-uniform heat transfer suppression to enhance PCM melting by angled fins. Appl Therm Eng 2018;129:269–79. https://doi.org/10.1016/j.applthermaleng.2017.10.030.
[39] Ji C, Qin Z, Dubey S, Choo FH, Duan F. Simulation on PCM melting enhancement with double-fin length arrangements in a rectangular enclosure induced by natural convection. Int J Heat Mass Tran 2018;127:255–65. https://doi.org/10.1016/J.IJHEATMASSTRANSFER.2018.07.118.
[40] Hosseinizadeh SF, Tan FL, Moosania SM. Experimental and numerical studies on performance of PCM-based heat sink with different configurations of internal fins. Appl Therm Eng 2011;31:3827–38. https://doi.org/10.1016/j.applthermaleng.2011.07.031.
[41] Biwole PH, Groulx D, Souayfane F, Chiu T. Influence of fin size and distribution on solid-liquid phase change in a rectangular enclosure. Int J Therm Sci 2018;124:433–46. https://doi.org/10.1016/j.ijthermalsci.2017.10.038.
[42] Kamkari B, Shokouhmand H, Bruno F. Experimental investigation of the effect of inclination angle on convection-driven melting of phase change material in a rectangular enclosure. Int J Heat Mass Tran 2014;72:186–200. https://doi.org/10.1016/j.ijheatmasstransfer.2014.01.014.
[43] Shokouhmand H, Kamkari B. Experimental investigation on melting heat transfer characteristics of lauric acid in a rectangular thermal storage unit. Exp Therm Fluid Sci 2013;50:201–12. https://doi.org/10.1016/j.expthermflusci.2013.06.010.
[44] Voller VR, Prakash C. A fixed grid numerical modelling methodology for convection-diffusion mushy region phase-change problems. Int J Heat Mass Tran 1987;30:1709–19.
[45] Safari V, Abolghasemi H, Kamkari B. Experimental and numerical investigations of thermal performance enhancement in a latent heat storage heat exchanger using bifurcated and straight fins. Renew Energy 2021;174:102–21. https://doi.org/10.1016/J.RENENE.2021.04.076.
[46] Safari V, Abolghasemi H, Darvishvand L, Kamkari B. Thermal performance investigation of concentric and eccentric shell and tube heat exchangers with different fin configurations containing phase change material. J Energy Storage 2021;37:102458. https://doi.org/10.1016/j.est.2021.102458.
[47] Karami R, Kamkari B. Investigation of the effect of inclination angle on the melting enhancement of phase change material in finned latent heat thermal storage units. Appl Therm Eng 2019;146:45–60. https://doi.org/10.1016/j.applthermaleng.2018.09.105.